

Observation of condensed moiré exciton polaritons in twisted photonic lattices at room temperature

Chunzi Xing,¹ Yu Wang,² Tobias Schneider,³ Xiaokun Zhai,¹ Xinzheng Zhang,² Haitao Dai,¹ Xiao Wang,⁴ Anlian Pan,⁴ Zhenyu Xiong,⁵ Hao Wu,⁵ Yuan Ren,⁵ Stefan Schumacher,^{3,6,7} Xuekai Ma,³ and Tingge Gao¹

¹*Department of Physics, School of Science, Tianjin University, Tianjin 300072, China*

²*The MOE Key Laboratory of Weak-Light Nonlinear Photonics and*

International Sino-Slovenian Joint Research Center on Liquid Crystal Photonics,

TEDA Institute of Applied Physics and School of Physics, Nankai University, Tianjin 300457, China

³*Department of Physics and Center for Optoelectronics and Photonics Paderborn (CeOPP),
Universität Paderborn, 33098 Paderborn, Germany*

⁴*College of Materials Science and Engineering, Hunan University, Changsha 410082, China*

⁵*Lab of quantum detection and awareness, Space Engineering University Beijing 101416, China*

⁶*Institute for Photonic Quantum Systems (PhoQS),
Paderborn University, 33098 Paderborn, Germany*

⁷*Wyant College of Optical Sciences, University of Arizona, Tucson, AZ 85721, USA*

Moiré lattices attract significant attention in double-layer graphene and TMD layer heterostructures as well as in photonic crystals due to the interesting exotic physics that emerges within these structures. However, direct measurement of the moiré ground, excited states and Bloch bands in twisted photonic lattices is still illusive. In this work we report strong coupling between excitons in CsPbBr₃ microplates and moiré photonic modes at room temperature. Depending on the coupling strength between the nearest potential sites, we observe staggered moiré polariton ground states, excited states and moiré polariton bands. Phase locked moiré zero (in-phase) states and moiré π (antiphase) states with different spatial distributions are measured. The moiré polariton distribution can be tuned into the shape of a parallelogram by controlling the depth and width of the potential in one photonic lattice with another superimposed one fixed. In addition, moiré polaritons in twisted 2D honeycomb lattices are also observed. Increasing the pumping density, we realize exciton polariton condensation in the moiré potential sites of the 1D/2D twisted lattices with the coherence time of around 1.4 ps. Our work lays the foundation to study coherent moiré polariton condensation in twisted photonic lattices at room temperature.

Moiré lattices in graphene bilayer and TMD monolayer heterostructures offer a tunable platform where the interlayer coupling of electrons and excitons leads to a plethora of physical phenomena, for example, the transition from superconductor to Mott insulator [1], observation of the quantum Hall effect [2] and nontrivial gauge field [3], the appearance of moiré excitons [4–6], and emergence of correlated exciton insulators [7–9]. On the other hand, the bands resulting from the coupling between potential sites arranged on a moiré lattice have been extended to photonic systems. In these systems, the localization and delocalization of light and nonlinear optical solitons can be observed by adjusting one photonic lattice against a second one into a particular angle [10]. The period of the moiré lattice in these twisted photonic structures can reach the size of several microns, thus the bands due to the coupling between the moiré potentials can be probed within several μm^{-1} in angle-resolved spectroscopy. In this case, both the momentum space and real space images can be directly measured. For example, photonic bands in the optical frequency range are probed in a double photonic crystals [11]. Cold atom condensates loaded in twisted photonic lattices have also been realized and the transition from superfluid to Mott insulator in the created moiré lattice is shown [12].

However, direct measurement of the moiré ground

state, excited states and moiré band states remain unexplored in the normal twisted photonic lattices. The observation of these modes can be used to investigate distinct state distribution in the momentum and real space resulted from different coupling strength among the moiré potentials. In addition, phase locking between different potential sites can be observed in the moiré bands. For example, the phase synchronization within a moiré flat band can enhance the performance of nanocavity laser array greatly [13]. On the other hand, π phase locking at the top of the moiré ground bands and bottom of the moiré excited bands will lead to different mode distribution compared to the ground band, which offers to study quantum simulation with tunable phase modulation. These π phase locked moiré states have not been observed yet.

As a quasiparticle due to the strong coupling between the exciton and photon mode [14] in Fabry-Perot microcavity, exciton polaritons can demonstrate similar Bose-Einstein condensation process as the cold bosonic particles at much higher temperature due to the very light effective mass and large exciton binding energy [15–17]. More importantly, exciton polaritons allow to investigate different phase locking when they are loaded into a photonic lattice [18]. To observe phase locking of zero and π of exciton polaritons in the moiré lattice at room tem-

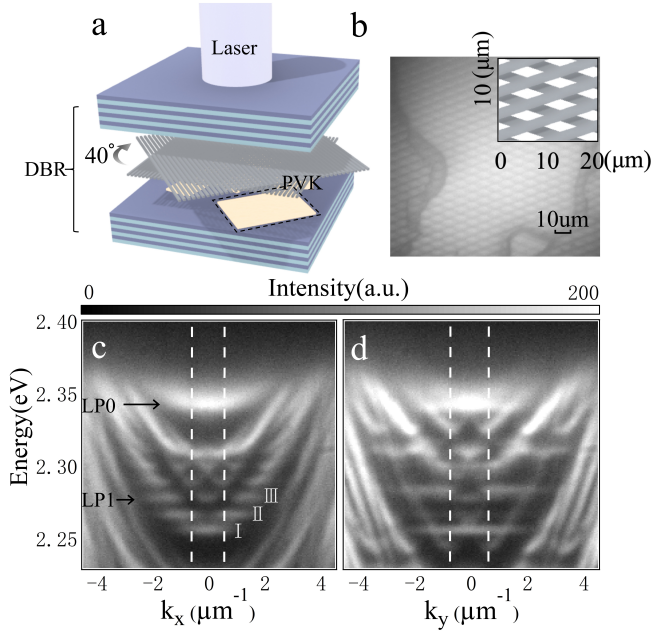


FIG. 1. **Schematics of the microcavity and photoluminescence exciton polariton dispersions in the moiré lattice.**(a) The structure of the microcavity. (b) The optical image of the twisted photonic structures, the right panel is the zoomed schematic of the moiré pattern. Photoluminescence dispersion along (c) k_x and (d) k_y direction. The dash lines indicate the edge of the first Brillouin zones. Moiré ground state (I), excited state (II) and moiré ground bands (III) are labeled in (c).

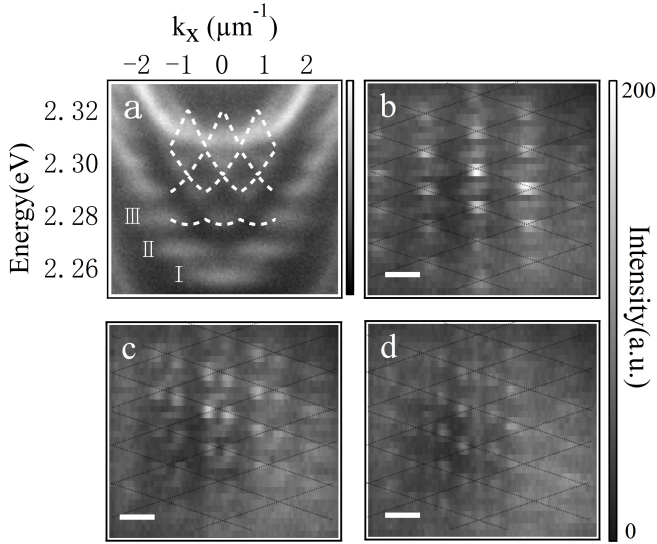


FIG. 2. **Moiré exciton polariton patterns with different energies.** (a) Zoomed dispersions along k_x with simulated dashed lines. Moiré ground state (I), excited state (II) and moiré ground bands (III) are labeled. (b-d) Moiré polariton spatial distributions of the ground state (I), the first excited state (II) and ground band states (III) labeled in Figure 2(a). The dash lines represent two photonic lattices. Scale bars in (b-d): $5 \mu\text{m}$.

perature, specific semiconductor materials with robust excitons and easy integration with photonic structures are needed, among which the perovskite CsPbBr_3 microplates stand out with large exciton binding energy and oscillator strength [19–24].

In the present work we realize strong coupling between the excitons of the CsPbBr_3 microplates and moiré photonic modes in twisted 1D/2D photonic lattice at room temperature, and observe exciton polariton condensation in the moiré potential traps. These lattices are composed of two tilted one (two) dimensional lattices fabricated within the microcavity. In our work, the moiré exciton polariton zero state and π state in these twisted photonic lattices are measured directly. The staggered moiré polaritons with different energies are either confined in the potential trap or in the potential barrier region. By modifying the potential trap depth and width of one photonic lattice which results in a moiré lattice in the shape of parallelograms, moiré polaritons with the distribution of localized dots, dimers and extended lines are observed due to the sensitivity against disorder. Furthermore, we demonstrate and realize the extension of strong coupling between excitons and moiré photonic bands in twisted 2D honeycomb lattices. The polariton condensation occurs in the 1D/2D moiré potential sites with the coherence time measured. Our work gives clear experimental evidence of phase locked moiré polaritons and condensation at room temperature, and paves the way for future investigations into room temperature quantum simulation in moiré photonic structures.

The microcavity is fabricated by transferring the chemical vapor deposition (CVD) grown CsPbBr_3 microplates onto the bottom DBR. Firstly, we discuss the interaction of excitons with twisted 1D photonic lattices, where the 1D photoresist lattice with the period of $4 \mu\text{m}$ (duty cycle: 50:50) and the thickness of 200 nm is formed by using the lithography technique onto the top of perovskite microplates (A layer of SiO_2 is deposited onto the perovskite for protection, detail is shown in SM). Another 1D photoresist lattice with the same duty cycle and depth is formed onto the top DBR with the angle of 40° against the bottom DBR. The microcavity is fabricated by pasting the top DBR against the bottom DBR with an air gap of around $3 \mu\text{m}$, as shown in Figure 1(a), where the moiré stripes consist of periodic rhombus arrays along horizontal (x) and vertical (y) direction. The optical image of the CsPbBr_3 microplate with the twisted moiré potential lattice is shown in Figure 1(b). The parameters of the rhombus are shown in the right panel of Figure 1(b), which induces different periodicities along x and y directions.

In the experiments, we place the sample such that the moiré pattern is along the x direction (the long symmetry axis of the rhombus is along the y direction). The energy (E) vs wavevector (k_x) dispersion of the microcavity is measured by using a home-made angle resolved

spectroscopy. The pumping source is a femtosecond laser (5700 Hz) with the wavelength of around 400 nm and pulse width of 130 fs. The pumping spot size of the laser is around $40 \mu\text{m}$ which covers around 8 periods of the moiré lattice. The dispersion along k_x direction is shown in Figure 1(c). Firstly, we note that there exist several sets of lower branch polaritons (for simplicity, we only plot LP0 and LP1 in Figure 1(c), a larger-energy-range dispersion is plotted in the SM) thanks to the long cavity length where multiple cavity modes strongly couple with the exciton resonance in the perovskite microplates at 2.43 eV. The strong coupling is confirmed at the large wavevector region where the dispersions are clearly bent when approaching the exciton resonance. Other modes with steeper curvatures come from the leakage of photons out of the perovskites or the luminescence from the photoresist.

The size of the Brillouin zone is reversely proportional to the period of the 1D potential lattice. The dispersion along k_y direction is shown in Figure 1(d). Due to different periods along x and y direction of the moiré lattice, the polariton bands show clear different periodicities and amplitudes in Figure 1(c) and Figure 1(d). The change in the size of the first Brillouin zone (from $1.10 \mu\text{m}^{-1}$ to $1.29 \mu\text{m}^{-1}$) due to different periods along these two directions (from $5.74 \mu\text{m}$ to $4.89 \mu\text{m}$) confirms the existence of the coupling between the moiré potential traps along the x direction.

In addition, in our microcavity, the depth of the moiré potential site is around 20 meV, where we observe both the discrete energy levels (the ground state at 2.26 eV, first excited state at 2.27 eV) and the band structure (annotated in Figure 1(c)) along k_x direction for polariton branch LP1. Within this branch, the discrete energy levels are formed due to small overlap of the lower-energy state between moiré potential traps, and polariton bands originate from larger overlap of the higher-energy modes among the moiré potential sites. The discrete polariton energy levels and bands are invisible in LP0 due to much smaller photon components.

Thanks to the coupling between the moiré sites, we observe a band gap opening between the ground band and excited band in Figure 1(c) (the ground band structure is invisible due to limited resolution). We fit the band structure of the moiré lattices and plot the simulated bands in Figure 2(a) which agree very well with the experimental results. Our simulation also shows the relation between the coupling strength among the moiré sites and the band gap opening between the moiré ground band and excited band, as discussed in SM. Similar band opening is observed for another lower polariton branch (shown in SM).

To check the existence of the moiré patterns, we measure the energy-resolved polariton distribution in real space. Firstly we show the moiré patterns corresponding to the ground state and the first excited states, which

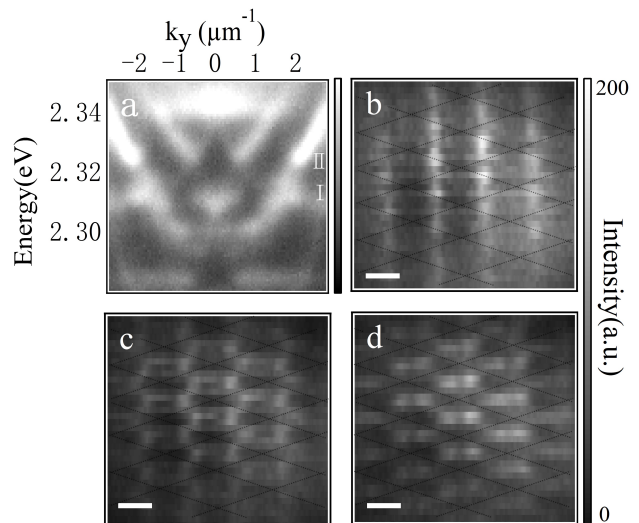


FIG. 3. **Phase locked moiré polariton patterns.** (a) Zoomed dispersions along k_y direction. Band I and II are labeled. (b-d) Moiré polariton spatial distributions at the bottom of band 1, the top of band I and the bottom of band II shown in Figure 3(a). The dash lines represent two photonic lattices. Scale bars in (b, d): $5 \mu\text{m}$.

are plotted in Figure 2(b-c). In these graphs, we can observe clear moiré states with different patterns along x direction. These modes are confined in the single moiré potential traps, where the ground states have a Gaussian shape (the emission at the barrier region comes from the bands from LP2, as shown in the SM), and the first excited modes are two-lobe states with the orientation along x direction. Due to small overlap between these states trapped in the single moiré sites, the dispersions corresponding to these modes are discrete energy levels. The real space image of the modes with a larger energy (2.28 eV) is plotted in Figure 2(d) which corresponds to the moiré ground band along k_x direction. This mode consists of three lobes along x direction and promises larger coupling between the nearest potential traps. With higher energy, moiré excited bands are observed along k_x direction in Figure 1(c) and Figure 2(a).

On the other hand, the band gap opening is also clearly observed along k_y direction, as shown in Figure 1(d) and Figure 3(a). The moiré polariton modes at the bottom (top) state of the band I and the bottom state of the band II shown in Figure 3(a) are plotted in Figure 3(b, c, d) (the two bands correspond to the ground and excited band along k_y direction). From these, we find clear zero and π phase locking of these high-energy modes across the moiré polariton lattice. Note that the zero state appears when the phase difference of polaritons in the moiré lattice is zero, which will give nonzero intensity distribution with the wavevector of $k_y = \pm m\pi/a$ (where m is an even integer). On the other hand, the π state can be observed with the wavevector of $k_y = \pm n\pi/a$ (where n is

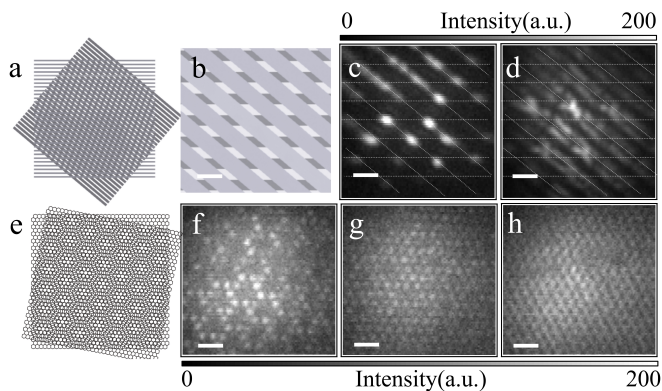


FIG. 4. **Moiré polariton patterns in a modulated 1D and twisted 2D photonic lattice.** (a) Schematics of the moiré pattern in modulated 1D lattices. (b) The zoomed image of the modulated 1D twisted photonic lattice. (c, d) The spatial distribution of the moiré polariton ground state and excited state. (e) Schematics of the moiré pattern in twisted 2D lattices. (f-h) The spatial distribution of the moiré polariton ground state, and higher excited states, with the dispersion shown in SM. Scale bars in (b-d, f-g): $5 \mu\text{m}$.

an odd integer) [18]. At the energy of 2.30 eV which corresponds to the zero state located at the bottom of band I with the wavevector of 0 and $\pm 1.1 \mu\text{m}^{-1}$, Figure 3(b) shows a clear moiré pattern along the y direction. In Figure 3(c) and (d) we can observe different moiré patterns at the top of the band I and the bottom of band II (the energy of these two states are 2.31 eV and 2.32 eV with the wavevector of $\pm 0.55 \mu\text{m}^{-1}$ and $\pm 1.65 \mu\text{m}^{-1}$), which is the π state. In above moiré zero state, the polaritons are visible in both the potential trap and barrier of the moiré lattice due to finite overlap of the wavefunctions, as plotted in Figure 3(b). Whereas the moiré π states shown in Figure 3(c) and Figure 3(d) are composed of a higher energy mode showing a staggered pattern. More importantly, these states are mainly located at the barrier region of the moiré lattice with the same periodicity as the low-energy modes in Figure 2(b-d).

Above moiré polaritons are robust against the disorders. In SM we show the spatial modes of the moiré ground state, excited state and moiré bands at other positions. Although distorted partly due to the inhomogeneity within the microcavity, they still keep the structure inherited from the moiré lattice, the phase locked polariton distributions in the moiré bands are similar as Figure 2 and Figure 3.

The moiré polaritons can be engineered quite easily within our photonic structures. In the twisted 1D lattices, the energy depth and width of the moiré potential sites can be tuned by modifying the parameters of one photonic lattice. In this case, different moiré polariton states can be observed directly. We replace the photorealist lattice on the perovskite microplate with a PMMA layer (thickness: 230 nm) and fabricate the photonic lat-

tice (period: $4 \mu\text{m}$, potential trap: $1.6 \mu\text{m}$, potential barrier: $2.4 \mu\text{m}$, depth: 50 nm) by using laser direct writing technique. In the new structures, the moiré polariton ground state distribution is in the shape of a parallelogram (Figure 4(a, b)). Due to lower potential trap depth of the PMMA photonic lattice, these moiré polaritons are fragile against defects or disorder due to lower energy and become deformed with random distribution, for example, localization trapped in the moiré potential, dimers, or delocalized lines, as shown in Figure 4(c). Excited and free moiré polariton modes in Figure 4(d) are robust against disorder in the shape of delocalized lines along the direction of the top photonic lattice (Polariton spatial modes at another position is shown in SM). In addition, our experimental scheme to observe moiré polaritons can be extended to twisted 2D lattices. To realize this, we fabricate a 2D honeycomb lattice onto the top of the perovskite microplates and the top DBR. With the twisting angle of 11° as shown in Figure 4(e), we can observe different moiré polariton patterns as shown in Figure 4(f-h) (the dispersions plotted in the SM). The observation of these tunable moiré polaritons enables studies of novel polariton phase transitions at room temperature in future works.

Finally, exciton polariton condensation can be realized in above 1D/2D twisted photonic lattices by increasing the pumping density. In Figure 5(a, e) we plot the integrated intensity and linewidth of polariton modes against the pumping density of the 1D/2D twisted lattices, which show polariton condensation occurs at around $11.5 \mu\text{J}/\text{cm}^2$ (1D) and $12 \mu\text{J}/\text{cm}^2$ (2D). In the two lattices, polaritons condense at the ground state of LP0 (Figure 5(b, f)) and are confined at the moiré potential traps in the 1D/2D photonic lattices, which are shown in Figure 5(c, g). We find the coherence time of the polaritons condensate in the two twisted lattices is around 1.4 ps, which is obtained by measuring the first-order temporal coherence $g^{(1)}(\tau)$ [29], plotted in Figure 5(d, h).

Compared with exciton polaritons loaded into periodic photonic lattices by etching pillars or growing buried mesa arrays [26, 27] in GaAs microcavity and moiré exciton polaritons based on TMD monolayer heterostructures at low temperature [28], we can directly measure the moiré polariton ground state, moiré excited state, moiré polariton bands and moiré polariton condensation at room temperature. This allows to observe how the moiré polaritons are manipulated by the periodicity, the potential depth and other parameters much more easily.

To summarize, we observe strong coupling between excitons of CsPbBr_3 microplates and moiré photonic bands of 1D (2D) twisted lattice in a microcavity at room temperature. Different moiré polariton stripes corresponding to the discrete energy levels and the continuous bands are observed. Moiré polariton condensation in the 1D/2D lattices is shown and coherence time is measured. The

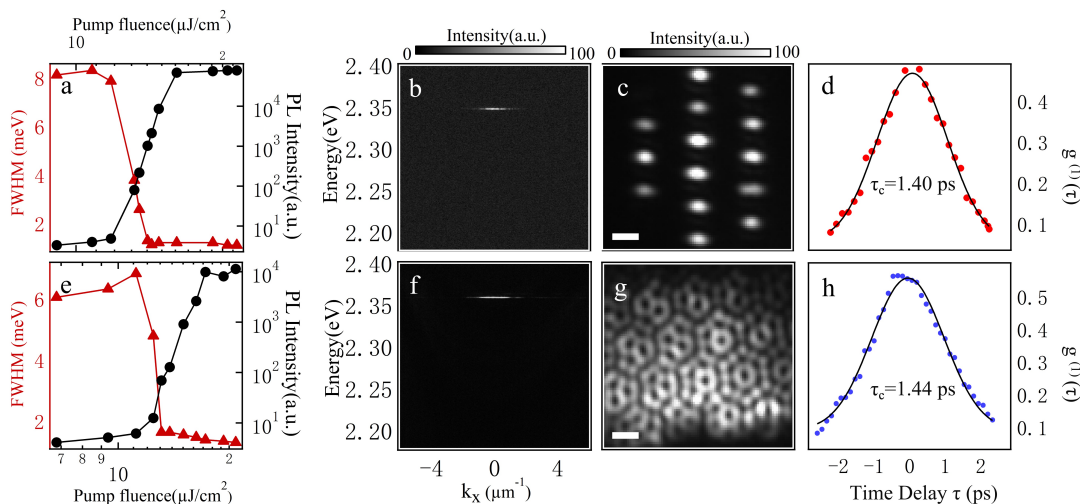


FIG. 5. **Moiré polariton condensation in twisted 1D/2D photonic lattices.** (a, e) Integrated intensity and linewidth of the moiré polaritons against the pumping density in twisted 1D(a)/2D(e) lattices. (b, c, f, g) Dispersion and real space images of the moiré polariton condensate in 1D(b, c)/2D(f, g) lattices, scale bars in (c, g): $5 \mu\text{m}$. (d, h) The first-order temporal coherence $g^{(1)}(\tau)$ of 1D(d) and 2D(h) photonic lattice.

realization of moiré polariton arrays with different phase locking can be used to investigate quantum phase transitions between the superfluid and Mott insulators in twisted photonic lattices at room temperature in the future.

T.Gao acknowledges the support from the National Natural Science Foundation of China (NSFC, No. 12174285, 12474315), especially T.Gao wants to thank Yongyou Zhang and Yang Yang for fruitful discussion. The Paderborn group acknowledges support from the German Research Foundation (DFG, No. 519608013). H.Dai thanks the National Natural Science Foundation of China (NSFC, No. 62375200).

[1] Y. Cao, V. Fatemi, S. Fang, K. Watanabe, T. Taniguchi, E. Kaxiras, and P. Jarillo-Herrero, Unconventional superconductivity in magic-angle graphene superlattices. *Nature* **556**, 43 (2018).

[2] C.R. Dean, L. Wang, P. Maher, C. Forsythe, F. Ghahari, Y. Gao, J. Katoch, M. Ishigami, P. Moon, M. Koshino, T. Taniguchi, K. Watanabe, K.L. Shepard, J. Hone, and P. Kim, Hofstadters butterfly and the fractal quantum Hall effect in moiré superlattices. *Nature* **497**, 598-602 (2013).

[3] P. San-Jose, J. González, and F. Guinea, Non-abelian gauge potentials in graphene bilayers. *Physical Review Letters* **108**, 216802 (2012).

[4] E.M. Alexeev, D.A. Ruiz-Tijerina, M. Danovich, M.J. Hamer, D.J. Terry, P.K. Nayak, S. Ahn, S. Pak, J. Lee, J.I. Sohn, M.R. Molas, M. Koperski, K. Watanabe, T. Taniguchi, K.S. Novoselov, R.V. Gorbachev, H.S. Shin, V.I. Fal'ko, and A.I. Tartakovskii, Resonantly hybridized excitons in moiré superlattices in van der Waals het-

erostructures. *Nature* **567**, 81–86 (2019).

[5] K.L. Seyler, P. Rivera, H. Yu, N.P. Wilson, E.L. Ray, D.G. Mandrus, J. Yan, W. Yao, and X. Xu, Signatures of moiré-trapped valley excitons in MoSe₂/WSe₂ heterobilayers. *Nature* **567**, 66–70 (2019).

[6] C. Jin, E.C. Regan, A. Yan, M. Iqbal Bakti Utama, D. Wang, S. Zhao, Y. Qin, S. Yang, Z. Zheng, S. Shi, K. Watanabe, T. Taniguchi, S. Tongay, A. Zettl, and F. Wang, Observation of moiré excitons in WSe₂/WS₂ heterostructure superlattices. *Nature* **567**, 76–80 (2019).

[7] Y. Cao, V. Fatemi, A. Demiri, S. Fang, S. L. Tomarken, J.Y. Luo, J.D. Sanchez-Yamagishi, K. Watanabe, T. Taniguchi, E. Kaxiras, R.C. Ashoori, and P. Jarillo-Herrero, Correlated insulator behaviour at half-filling in magic-angle graphene superlattices. *Nature* **556**, 80 (2018).

[8] H. Li, S. Li, M.H. Naik, J. Xie, X. Li, J. Wang, E. Regan, D. Wang, W. Zhao, S. Kahn, K. Yumigeta, M. Blei, T. Taniguchi, K. Watanabe, S. Tongay, A. Zettl, S.G. Louie, F. Wang, and M.F. Crommie, Imaging moiré flat bands in three-dimensional reconstructed WSe₂/WS₂ superlattices. *Nature Materials* **20**, 945–950 (2021).

[9] R. Xiong, J.H. Nie, S.L. Brantly, P. Hays, R. Sailus, K. Watanabe, T. Taniguchi, S. Tongay, and C. Jin, Correlated insulator of excitons in WSe₂/WS₂ moiré superlattices. *Science* **368**, 860-864 (2023).

[10] P. Wang, Y. Zheng, X. Chen, C. Huang, Y.V. Kartashov, L. Torner, V.V. Konotop, and F. Ye, Localization and delocalization of light in photonic moiré lattices. *Nature* **577**, 42-46(2019).

[11] H. Tang, B. Lou, F. Du, M. Zhang, X. Ni, W. Xu, R. Jin, S. Fan, and E. Mazur, Experimental probe of twist angle-dependent band structure of on-chip optical bilayer photonic crystal. *Science Advances* **9**, eadh8498 (2023).

[12] Z. Meng, L. Wang, W. Han, F. Liu, K. Wen, C. Gao, P. Wang, C. Chin, and J. Zhang, Atomic Bose-Einstein condensate in twisted-bilayer optical lattices. *Nature* **615**, 231–236 (2023).

- [13] H. Luan, Y. Ouyang, Z. Zhao, W. Mao, and R. Ma, Reconfigurable moiré nanolaser arrays with phase synchronization. *Nature* **624**, 282–288 (2023).
- [14] A. Kavokin, J.J. Baumberg, G. Malpuech, and F.P. Laussy, *Microcavities* (OUP Oxford, 2007).
- [15] J. Kasprzak, M. Richard, S. Kundermann, A. Baas, P. Jeambrun, J.M.J. Keeling, F.M. Marchetti, M.H. Szymańska, R. André, J.L. Staehli, V. Savona, P.B. Littlewood, B. Deveaud, and L.S. Dang, Bose–Einstein condensation of exciton polaritons. *Nature* **443**, 409–414 (2006).
- [16] R. Balili, V. Hartwell, D. Snoke, L. Pfeiffer, and K. West, Bose–Einstein condensation of microcavity polaritons in a trap. *Science* **316**, 1007–1010 (2007).
- [17] S. Christopoulos, G. Baldassarri Höger von Högersthal, A.J.D. Grundy, P.G. Lagoudakis, A.V. Kavokin, J.J. Baumberg, G. Christmann, R. Butté, E. Feltn, J.-F. Carlin, and N. Grandjean, Room-Temperature polariton lasing in semiconductor microcavities. *Physical Review Letters* **98**, 126405 (2007).
- [18] C.W. Lai, N.Y. Kim, S. Utsunomiya, G. Roumpos, H. Deng, M.D. Fraser, T. Byrnes, P. Recher, N. Kumada, T. Fujisawa, and Y. Yamamoto, Coherent zero-state and pi-state in an exciton–polariton condensate array. *Nature* **450**, 529–532 (2007).
- [19] Y. Li, X. Ma, X. Zhai, M. Gao, H. Dai, S. Schumacher, and T. Gao, Manipulating polariton condensates by Rashba-Dresselhaus coupling at room temperature. *Nature Communications* **13**, 3785 (2022).
- [20] X. Zhai, X. Ma, Y. Gao, C. Xing, M. Gao, H. Dai, X. Wang, A. Pan, S. Schumacher, and T. Gao, Electrically controlling vortices in a neutral exciton-polariton condensate at room temperature. *Physical Review Letters* **131**, 136901 (2023).
- [21] Y. Gao, X. Ma, X. Zhai, C. Xing, M. Gao, H. Dai, H. Wu, T. Liu, Y. Ren, X. Wang, A. Pan, W. Hu, S. Schumacher, and T. Gao, Single-shot spatial instability and electric control of polariton condensates at room temperature. *Physical Review B* **108**, 205303 (2023).
- [22] H. Li, Q. Ai, Y. Li, X. Zhai, T. Liu, Y. Ren, and T. Gao, Localization of anisotropic exciton polariton condensates in perovskite microcavities. *Applied Physical Letters* **120**, 011104 (2022).
- [23] M.S. Spencer, Y. Fu, A.P. Schlaus, D. Hwang, Y. Dai, M.D. Smith, D.R. Gamelin, and X.-Y. Zhu, Spin-orbit-coupled exciton-polariton condensates in lead halide perovskites. *Science Advances* **7**, eabj7667 (2021).
- [24] R. Su, J. Wang, J. Zhao, J. Xing, W. Zhao, C. Diederichs, T.C.H. Liew, and Q. Xiong, Room temperature long-range coherent exciton polariton condensate flow in lead halide perovskites. *Science Advances* **4**, eaau0244 (2018).
- [25] Y. Wang, Y. Lan, Q. Song, F. Vogelbacher, T. Xu, Y. Zhan, M. Li, W.E.I. Sha, and Y. Song, Colorful efficient moiré-perovskite solar cells. *Advanced Materials* **33**, 2008091 (2021).
- [26] F. Baboux, L. Ge, T. Jacqmin, M. Biondi, E. Galopin, A. Lemaitre, L. Le Gratiet, I. Sagnes, S. Schmidt, H.E. Türeci, A. Amo, and J. Bloch, Bosonic condensation and disorder-induced localization in a flat band. *Physical Review Letters* **116**, 066402 (2016).
- [27] C.E. Whittaker, E. Cancellieri, P.M. Walker, D.R. Gulevich, H. Schomerus, D. Vaitiekus, B. Royall, D.M. Whittaker, E. Clarke, I.V. Iorsh, I.A. Shelykh, M.S. Skolnick, and D.N. Krizhanovskii, Exciton polaritons in a two-dimensional Lieb lattice with spin-orbit coupling. *Physical Review Letters* **120**, 097401 (2018).
- [28] L. Zhang, F. Wu, S. Hou, Z. Zhang, Y.H. Chou, K. Watanabe, T. Taniguchi, S.R. Forrest, and H. Deng, Van der Waals heterostructure polaritons with moiré-induced nonlinearity. *Nature* **591**, 61–65 (2021).
- [29] D. Xu, W. Xie, W. Liu, J. Wang, L. Zhang, Y. Wang, S. Zhang, L. Sun, X. Shen, Z. Chen, Polariton lasing in a ZnO microwire above 450 K. *Applied Physical Letters* **104**, 082101 (2014).